Metallomics, 0, 2021, mfab051
https://doi.org/10.1093/mtomcs/mfab051
Advance access publication date: 17 August 2021
Paper

Synchrotron fluorescence imaging of individual mouse beta-cells reveals changes in zinc, calcium, and iron in a model of low-grade inflammation

Kira G. Slepchenko[1,2,3], Si Chen[4], Grace P. Counts[1], Kathryn L. Corbin[3], Robert A. Colvin[1,2,*] and Craig S. Nunemaker[2,3,*]

[1]Department of Biological Sciences, Ohio University, Athens, Ohio, USA, [2]Molecular and Cellular Biology, Ohio University, Athens, Ohio, USA, [3]Department of Biomedical Sciences, Heritage College of Osteopathic Medicine, Ohio University, Athens, Ohio, USA and [4]Advanced Photon Source, Argonne National Laboratory, Lemont, Illinois, USA

*Correspondence: Department of Biomedical Sciences, Heritage College of Osteopathic Medicine, Ohio University, 228 Irvine Hall, Athens, OH 45701, USA. Emails: colvin@ohio.edu; nunemake@ohio.edu

Abstract

Pancreatic beta-cells synthesize and secrete insulin maintaining an organism's energy homeostasis. In humans, beta-cell dysfunction and death contribute to the pathogenesis of type 2 diabetes (T2D). Although the causes of beta-cell dysfunction are complex, obesity-induced low-grade systemic inflammation plays a role. For example, obese individuals exhibiting increased levels of proinflammatory cytokines IL-6 and IL-1beta have a higher risk of beta-cell dysfunction and T2D. Interestingly, obesity-induced inflammation changes the expression of several cellular metal regulating genes, prompting this study to examine changes in the beta-cell metallome after exposure to proinflammatory-cytokines. Primary mouse beta-cells were exposed to a combination of IL-6 and IL-1beta for 48 hours, were chemically fixed and imaged by synchrotron X-ray fluorescent microscopy. Quantitative analysis showed a surprising 2.4-fold decrease in the mean total cellular content of zinc from 158 ± 57.7 femtograms (fg) to 65.7 ± 29.7 fg; calcium decreased from 216 ± 67.4 to 154.3 ± 68.7 fg (control vs. cytokines, respectively). The mean total cellular iron content slightly increased from 30.4 ± 12.2 to 47.2 ± 36.4 fg after cytokine treatment; a sub-population of cells (38%) exhibited larger increases of iron density. Changes in the subcellular distributions of zinc and calcium were observed after cytokine exposure. Beta-cells contained numerous iron puncta that accumulated still more iron after exposure to cytokines. These findings provide evidence that exposure to low levels of cytokines is sufficient to cause changes in the total cellular content and/or subcellular distribution of several metals known to be critical for normal beta-cell function.

Keywords: beta-cells, type 2 diabetes, obesity, inflammation, diabetes, cytokines, interleukin-6 (IL-6), interleukin-1beta (IL-1beta), zinc, calcium, iron

Graphical abstract

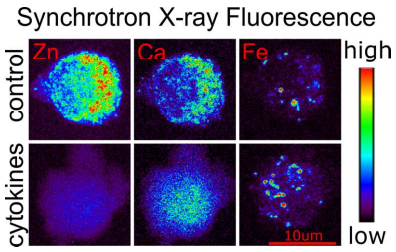

Introduction

Pancreatic beta-cells synthesize and secrete the hormone insulin, which regulates energy metabolism in organisms. The dysfunction and death of beta-cells contributes to the development of type 2 diabetes (T2D), a metabolic disease whose occurrence is steadily increasing worldwide. T2D affects more than 34 million individuals in the USA (>10% of the population), as reported in 2020.[1] To halt the worldwide increase in T2D, will require a better understanding of pancreatic beta-cell function under both normal physiological conditions and aberrant conditions associated with the development of T2D.

Obesity places metabolic stress on the body, which results in a state of chronic low-grade inflammation[2] and has been shown to be an important risk factor for developing T2D.[3,4] A number of proinflammatory cytokines are elevated in the general

Received: June 30, 2021. **Accepted:** August 2, 2021
© The Author(s) 2021. Published by Oxford University Press. All rights reserved. For permissions, please e-mail: journals.permissions@oup.com

circulation of obese individuals compared to lean individuals, including TNF-alpha, C-reactive protein (CRP), monocyte chemoattractant protein-1 (MCP-1), interleukin-1beta (IL-1beta), and interleukin-6 (IL-6).[3–9] In particular, IL-1beta and IL-6 appear to be specifically related to the development of T2D.[5] Combinations of cytokines at low levels have been shown to alter pancreatic islet calcium handling,[10–14] promote amyloid formation,[15] and disrupt cell-to-cell communication within the islets.[16,17] Circulating cytokines have been included among possible triggers of beta-cell inflammation seen in T2D.[18] However, the underlying cellular mechanisms leading to beta-cell dysfunction and death linked with chronic inflammation associated with the pathogenesis of T2D is not well understood.

It has become evident that inflammation causes changes in gene expression of many metal-regulating genes. For example, iron and copper metalloreductase—six transmembrane epithelial antigen of prostate (STEAP4)[19] has been shown to be highly upregulated after exposure to IL-6 and IL-1beta at concentrations found in obese individuals.[20] In addition, two other genes involved in iron regulation were upregulated: hepcidin and lipocalin.[20] Inflammation downregulates zinc transporter ZnT8,[21] zinc and iron transporter DMT1,[22] and calcium transporter SERCA.[10,23] Cytokines also upregulate iron and zinc transporter ZIP14.[24] We therefore hypothesized that the metallome of pancreatic beta-cells will be altered by exposure to obesity-induced cytokines IL-1beta and IL-6.

Synchrotron X-ray fluorescence microscopy (SXFM) can provide evidence to test the hypothesis, because it has the sensitivity and sub-micron resolution needed for precise measurements and visualization of the metallome of single primary beta-cells providing data on the total cellular content and subcellular distribution of zinc, calcium, and iron. SXFM has been successfully used to study normal and aberrant metal homeostasis in many cell types.[25] There is a recent report of whole islets metal contents with SXFM,[26] however the metallome of pancreatic beta-cells in primary culture has yet to be studied. The goals of this study are to (1) determine if SXFM can be used to study the metallome of individual beta-cells and (2) to investigate if exposure to cytokines IL-6 and IL-1beta, at circulating concentrations found in obese individuals, would result in measurable changes in either the total cellular content or subcellular distribution of metals, thus giving us clues as to the pathogenesis of T2D. This study was performed in beta-cells from male mice, and we found that a 48-h exposure to cytokines IL-6 and IL-1beta did indeed result in measurable changes to the beta-cell metallome.

Methods

Mouse pancreatic islets

The isolation of mouse pancreatic islets was performed as described previously.[27] Male CD-1 mice were used for this study (11 weeks of age). Before consequent digestion for monolayer, isolated islets were incubated at 37°C with 95% humidity and 5% CO_2 for 24 h in RPMI medium supplemented with 10% fetal bovine serum and 1% penicillin/streptomycin. Procedures utilizing animals were approved by the Ohio University Animal Care and Use Committee.

Preparation of silicon-nitrite windows for beta-cell attachment

Prior to visualization with SXFM, beta-cells were first allowed to attach to silicon-nitride windows (Norcada of Silson Ltd.). To prepare for cell attachment, windows were washed by dipping in deionized water, followed by 70% ethanol, and finally 100% ethanol. The windows were air dried and sterilized with UV for 30 min. The windows were next treated with 0.01% poly-D-Lysine (dissolved in sterile water) for 20 min at room temperature. The excess solution was aspirated after incubation, and windows were air dried overnight in a sterile culture hood.

Preparation of beta-cell monolayer

The pancreatic islets from three male CD-1 mice were pooled (about 33 islets per mouse, total about 100 islets for each condition). Islets were washed in phosphate-buffered saline (PBS) (prewarmed to 37°C) and transferred into siliconized glass tube with 500 μl of 0.05% trypsin EDTA (pre-warmed to 37°C). The chemical digestion was performed for 2 min at 37°C. To promote dissociation of the islets into single cells, forceful triturations were performed with a siliconized glass Pasteur pipette. The dissociation of the islets was monitored with a dissecting microscope, and the trituration continued until a minimal number of cell clumps were observed. The digestion was stopped by addition of 2ml of prewarmed complete RPMI medium. The cell suspension was spun at 1500 rpm (800 xg) for 6 min to pellet the cells. The cell pellet was resuspended in 80 μl of prewarmed RPMI medium. 10 μl of cell suspension was added to the center of the prepared windows. Each window was placed into one well of a 6-well plate and incubated at 37°C/5% CO_2 for 40 min, to promote cell attachment to the surface of the windows. After attachment was complete, 3 ml of prewarmed complete RPMI medium was gently added to each well. Successful cell attachment was approximately 40–50%. The cells attached to the windows were incubated for 24 h before the experimental treatments began. Before each treatment, windows with cells were observed to ensure cells remained attached and that the culture was contaminant free.

Cytokine exposure (low-grade inflammation)

The cytokine stocks were prepared in PBS with addition of 0.1% bovine serum albumin. The stocks were stored at −80°C. Before addition to the cells, the solutions were prepared in complete RPMI medium (prewarmed to 37°C). Control (untreated) cells were incubated in complete RPMI medium. The experimental cells were incubated with cytokines: 10 pg/ml IL-1beta and 20 pg/ml IL-6 in complete RPMI medium. To add the solutions to the cells, first the old medium was aspirated and the fresh complete RPMI medium was added to control cells and complete RPMI medium with cytokines was added to experimental cells. The total time of cytokine exposure was 48 h: the cells were incubated at 37°C/5% CO_2 for 24 h and fresh cytokines were added after 24 h. To confirm that an inflammatory state was induced in beta-cells, the expression level of inducible nitric oxide synthase (NOS2) was measured and found to be highly upregulated in cells after exposure to cytokines (Fig. S1). NOS2 is a marker of inflammation,[28] and the significant upregulation of NOS2 confirms that the low-grade inflammation model we are using results in inflammatory response in pancreatic beta-cells.

Chemical fixation of beta-cell monolayer after exposure to cytokines

After 48 h of experimental treatment, the windows were handled with forceps and first briefly washed by dipping in PBS. The PBS used during this step only was first pre-treated with Chelex (to remove adventitious metal contamination) and contained 100 μM EDTA,[29] to remove metals from the surface of the windows and attached cells.[29] All manipulations of windows were

UNCORRECTED PROOF

performed with extreme caution to not disturb the attached cells and to prevent damage to the windows. Cells were chemically fixed with 4% formaldehyde (EM-grade) in PBS (Chelex treated) for 20 min at room temperature. The chemical fixation was optimized to minimize the diffusion of metals from the cells (minimal washing of samples and minimal incubation with the fixative). After fixation, the cells were briefly rinsed three times in PBS. Dehydration of the attached beta-cells was performed as previously described.[30] The fixed and washed cells on the windows were gently handled with forceps and dipped twice in Tris-glucose solution (10 mM Tris base, 260 mM glucose, 9 mM acetic acid).[30] The windows were gently lifted from the solution and placed on bibulous paper. A small piece of absorbent wipes (Kim-wipes) was used to remove excess solution from the windows by touching the corners of the window's frame and letting the capillary action draw the solution away from the attached cells. The windows were placed in a desiccator overnight to allow the cells to slowly dehydrate.

There are multiple ways to prepare cells for SXFM, one of such methods is scanning cells frozen and hydrated.[31] Chemical fixation with different fixatives has been shown to result in changes to the metallome of cells.[32] To ensure that the fixation method we used did not cause significant disturbance of the beta-cell metallome we compared beta-cells that were scanned hydrated with the chemically fixed cells. The method of sample preparation, we used in this study, provided consistent and optimal preservation of cellular structure across all experimental treatments (Fig. S2). However, the steps involved in washing and chemical fixation may result in loss of cellular metals. At least for cellular zinc, calcium, and iron, loss was minimal based on comparisons with beta-cells scanned frozen and hydrated (Fig. S2 B–E). Although we are limited presently in the number of hydrated cells we could analyze, we found that for beta-cells, the distributions and total content of calcium, zinc, and iron are comparable between hydrated and chemically fixed cells (Fig. S2 A--E), demonstrating that the loss of metals due to sample preparation is minimal in this study. In addition, hydrated cells showed similar metal levels assessed after cytokine exposure when compared to chemically fixed cells (Fig. S2 A, F--I). Nevertheless, the possibility remains that there are changes in labile metal pools. On the other hand, the changes in labile pools are difficult to investigate with SXFM because labile pools represent a small fraction of the total metal content that is detected with SXFM. The changes in labile metal pools should be investigated with more suitable techniques.

Synchrotron X-ray fluorescence microscopy

After the overnight dehydration, the samples were packaged for shipping with a desiccator pouch inside an envelope. The samples were shipped overnight to Argonne National Laboratory and stored in a desiccator under vacuum for less than 1 week before scanning. SXFM measurements were performed at the Bionanoprobe (BNP), a hard X-ray scanning nanoprobe located at sector 9-ID-B of the Advanced Photon Source.[33] A double-crystal Si < 111 > monochromator was used to select 10.5 keV photons as incident beam. The photons were then focused to ~100 nm spot size using a pair of stacked zone plates. The scans were performed in fly-scan mode with 100 nm pixel size and 50–100 ms dwell time per pixel. X-ray fluorescence spectra were acquired using a Vortex-ME4 detector mounted at 90 degrees to the incident beam. The acquired spectra were normalized to the incident flux and fitted for elemental quantification.

A total of four windows with cells attached were scanned during one continuous beamline session (two windows per experimental treatment, 10–15 cells per window). The cells attached to the windows are a mix of cell types from the pancreatic islets (islets of Langerhans). Mouse islets contain 60–80% beta-cells, 10–20% alpha-cells, and less than 5% delta cells.[34] In culture, beta-cell populations are typically at 77–78%.[35] Because the beta-cells are the focus of the investigation, we scanned mostly cells that met the criteria of beta-cell morphology: round or oval shape and were approximately 13–15 μm in diameter. Cells larger than 18 μm in diameter and triangular were avoided. In addition, immunofluorescence was performed on cells after SXFM scanning with insulin-specific antibodies, which specifically labels beta-cells (data not shown).

Data analysis

MAPS software[36] (provided by Argonne National Laboratory) was used to fit the spectra and quantify the elemental content in each of the scan areas. A thin-film (RF8-200-S2453, AXO DRESDEN GmbH, Germany) was used as a standard sample for quantification calibration. Cellular images used for analysis and presentation purposes were captured and exported in .gif format using MAPS software. Prior to export, scanned images for each element were separately adjusted by setting the maximal intensity of the scale bar to the same value ($\mu g/cm^2$) across all the scanned images for that element (the exact max numbers are reported in the figure legends). The quantification of the total cellular content of the metals was performed with MAPS software, by using the regions of interest (ROI) function. Each cell was manually highlighted to be included in ROI, and the background was determined by outlining an ROI in a region without the cell. The resulting intensities were imported from MAPS to Excel. The background intensity was subtracted from the total cellular intensity. To compare subcellular metal densities in individual cells, MAPS line scan function was used, and the density of each metal is reported as a function of the position along that line. The figure graphs were generated with GraphPad Prism 8 software.

Identification and analysis of iron puncta with ImageJ

An unbiased method was developed to identify and analyze iron puncta using the open source image-analyzing software ImageJ.[37] A new ImageJ macro was created to standardize the identification of iron puncta (the code of the macro is added to supplemental materials, Table 1). The advantage of the ImageJ macro is that it simplifies the identification of puncta in individual cells and eliminates the need for laborious manual drawing of individual ROIs. Importantly, for data analysis, the macro eliminates experimenter errors and unintentional bias. The workflow of the ImageJ macro and examples of images and quantitative outputs can be found in Fig. S3.

Statistical analysis

The statistical analysis was performed with GraphPad Prism8. To identify outliers, all cells were subjected to robust regression followed by outlier identification method—ROUT.[38] Cells were removed from the data set if one of the elements was found to be an outlier; four cells were found to be outliers in the control group (16% of the sample); and four cells were found to be outliers in cytokine-treated group (14% of the sample). The resulting data set included 21 control (untreated) cells and 24 experimental cells (exposed to cytokines). The Shapiro–Wilk and Q-Q plots were used to test the normality. The equal variance was tested by Levene's test for homogeneity. The appropriate t-tests

UNCORRECTED PROOF

were used to assess the significance (Welch's t-test and two sample t-test, Kolmogorov--Smirnov t-test), $\alpha = 0.05$, P-value < 0.05 was considered significant. The t-test and statistics are reported for statistically significant results in the figure legends. In addition, GraphPad Prism8 was used to run Chi-square test for independence to compare the distribution of iron density in puncta to determine if the groups were related (control vs. after exposure to cytokines).

Results and discussion

Zinc is markedly depleted in pancreatic beta-cells after exposure to cytokines

A major finding of this study is that after 48 h of exposure to proinflammatory cytokines, mean total cellular zinc is depleted by more than 50% (2.4-fold decrease). The total zinc cellular content of control beta-cells was 158. ± 57.7 fg and 65.7 ± 29.7 fg after exposure to cytokines (mean ± S.D.) (Welch's t-test, t(28.9) = 6.65, $P < 0.0001$, N (control) = 21, N (cytokines) = 24) (Fig. 1E). The volume of beta-cells has been reported by Bock[39] at about 1300 μm^3, which is comparable to our estimates of the single beta-cells volume at 1361 ± 360 μm^3 in control and 1631 ± 550.3 μm^3 cells after exposure to cytokines. Using the total zinc content reported by SXFM and estimated volume of beta cells, the average zinc concentration in beta-cells is 1.87 ± 0.77 mM in control cells and about 0.66 ± 0.33 mM after exposure to cytokines. For comparison, this is more than 10 times higher than the average zinc concentration in neuronal soma reported to be 100–200 μM for a volume of 1000 μm^3. [40–42] Cytoplasmic zinc is present throughout the cell in either protein-bound or free forms. Free zinc levels have been studied extensively, due to the availability of fluorescent zinc probes, however free zinc constitutes a tiny fraction of total cellular zinc content and has been estimated to be about 400 pM in beta-cells,[43] which is ~0.00002% of our millimolar estimates of total cellular zinc.

Recently, a similar magnitude of zinc depletion was observed by Lawson, who used inductively coupled plasma mass spectrometry (ICP-MS) to measure total zinc content in cultured beta-cells (MIN6) and showed that after overstimulation with potassium chloride (KCl) cells exhibited 2.8-fold zinc depletion.[44] In addition zinc depletion resulted in downregulation of genes responsible for maintenance of beta-cell identity, suggesting that zinc depletion of this magnitude contributes to beta-cell de-differentiation.[44] For a long time glucotoxicity has been linked to beta-cell de-deffertiation,[45] however data reported by Lawson suggest that zinc depletion can cause beta-cell de-differentiation.[44] Using SXFM we show a comparable zinc depletion of 2.4-fold after exposure to cytokines. Labile zinc has been also shown to decrease following exposure to much higher and more lethal concentrations of cytokines,[46,47] however the labile zinc is a fraction of the total zinc content we are reporting with SXFM. An interesting avenue of further investigation can include the assessment of beta-cell identity transcriptome after exposure to obesity-induced cytokines. This is of great interest because beta-cell de-differentiation has been suggested in the progression of T2D.[48,49]

Subcellular zinc distribution in the beta-cell

Visual inspection of SXFM images show varying densities of zinc in the perinuclear region of the cells in a punctate pattern (Fig. 1A). The perinuclear space of the cell is occupied by insulin granules, as has been shown with electron microscopy,[50] and free zinc has been shown in insulin granules.[51,52] The perinuclear space is also occupied by Golgi apparatus[53] and endoplasmic reticulum (ER),[53] which have been shown to contain free zinc.[53] Thus, synchrotron X-ray fluorescence data from the present study are consistent with previous reports that zinc in addition to being found in the cytosol can be found highly concentrated in insulin granules, Golgi, and ER.[53]

An additional approach to illustrate zinc subcellular distribution is to employ the line scan function in MAPS software, which reports the density of the metal as a function of the position along the line (Fig. 1B). The line was drawn horizontally through the middle of the cell for analysis (line not shown to avoid obstructing the image). To facilitate a comparison of visual zinc distribution (Fig. 1A) and zinc density (Fig. 1B), the position of the line scan in Fig. 1B corresponds to the scale on top of the image in Fig. 1A. As expected, zinc distribution shown with a line scan, is consistent with highest zinc concentrations being localized to the perinuclear space. In contrast, zinc in cytokine-treated cells is uniformly distributed throughout the cytosol (Fig. 1A). The line scan of zinc density in cytokine-treated cell supports the visual observations of marked zinc depletion (Fig. 1B). The qualitative and quantitative analysis of SXFM data show that exposure to cytokines strikingly alters the distribution and mean total cellular content of zinc in beta-cells.

Calcium is decreased and its subcellular location altered in pancreatic beta-cells after exposure to cytokines

Cellular calcium is important for beta-cell function because it is required for insulin secretion.[54] Calcium also contributes to the endogenous pulsatility necessary for appropriate patterns of insulin release.[55] The subcellular distribution of calcium is noticeably changed after 48-h exposure to cytokines: the punctate pattern of calcium distribution is lost, and calcium appears to translocate, at least partially, from the perinuclear region to the nuclear region (Fig. 1A). As shown in Fig. 1C, the line scan data support the visual observations that calcium concentrations appear to be highest in presumed nuclear region of the cytokine-treated cell, consistent with the location of the nucleus, suggesting substantial cytokine-induced nuclear localization of calcium. The total calcium cellular content of control beta-cells was 216 ± 67.4 fg and after exposure to cytokines was decreased to 154.3 ± 68.7 fg (mean ± S.D.), (Two sample t-test, t(43) = 3.040, $P = 0.0040$, N (control) = 21, N (cytokines) = 24) (Fig. 1F). The qualitative and quantitative analysis of SXFM data show that exposure to cytokines alters the distribution and density of calcium in beta-cells.

The perinuclear calcium is likely contained in the ER since the ER is typically perinuclear in beta-cells and the ER stores a large proportion of cellular calcium.[56] The loss of perinuclear calcium is consistent with previous reports that exposure to cytokines leads to decrease in ER calcium[10,23,57] and leads to changes to glucose-stimulated calcium responses in beta-cells.[11] Of note, modulating calcium homeostasis is being explored to prevent cytokine-mediated beta-cell death.[58] Studies of nuclear calcium in the beta-cell are limited, however, K_{ATP} channels in the nuclear envelope may play a key role in transducing nutrient-derived signals into the nucleus.[59] Further, the nuclear calcium response is much greater than that of the cytoplasm following stimulation by glucose or oleate,[59] which is consistent with our observations with cytokines. It is reasonable to suspect if these stressors can alter nuclear calcium signaling, then the cytokines involved with low-grade inflammation could as well.[11] As reviewed in Ramadan et al.,[60] raising nuclear calcium could activate important kinases,

UNCORRECTED PROOF

COLOUR ONLINE, B&W IN PRINT

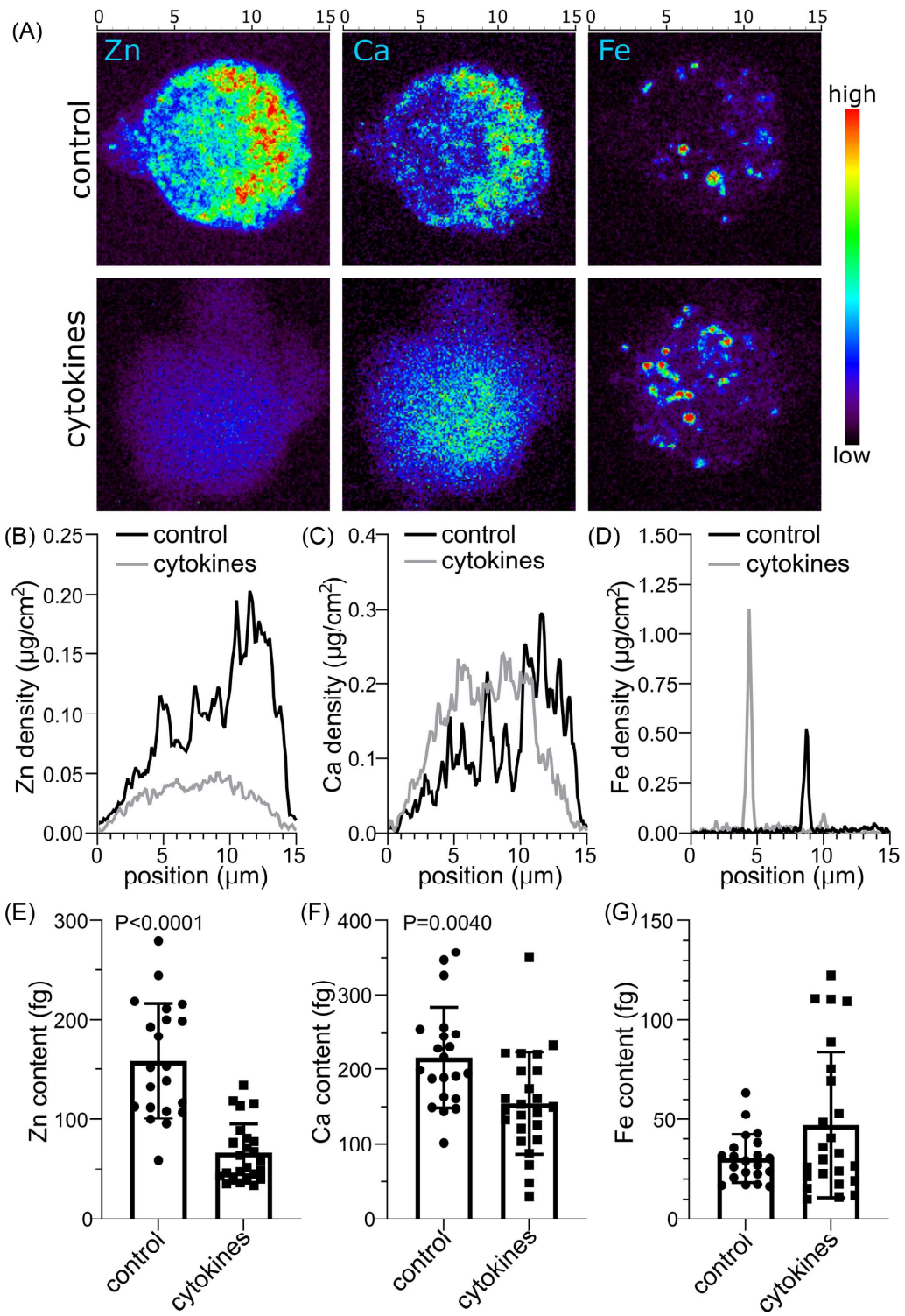

Fig. 1 Cytokine exposure alters the distribution and content of zinc, calcium, and iron in single pancreatic beta-cells as detected with synchrotron X-ray fluorescence microscopy. (A) Representative images of control beta-cell (untreated) and beta-cell exposed to cytokines (10 pg/ml IL-1beta and 20 pg/ml IL-6) for 48 h. Zinc (Zn) (max = 0.2 $\mu g/cm^2$), calcium (Ca) (max = 0.5 $\mu g/cm^2$), iron (Fe) (max = 0.25 $\mu g/cm^2$). Scale bar is 15 μm (top of the images). (B and C) The line scans represent the relative distributions of metals in the control beta-cells (black line) and beta-cells after exposure to cytokines (grey line). The line scan position is through the center of the cells. (D) The line scans through iron puncta with highest iron density. (E-G) Total metal content per cell (fg) for zinc (E), calcium (F), and iron (G). The columns represent means ± S.D. of all beta-cells. Each dot represents the value of an individual beta-cell (N (control) = 21, N (cytokines) = 24 for each metal). Different statistical tests were required based on results of normality and variance tests. Zinc (Welch's t-test, $t(28.9) = 6.65$, $P < 0.0001$); calcium (Two sample t-test, $t(43) = 3.040$, $P = 0.0040$); (Kolmogorov–Smirnov t-test, $P = 0.2965$, $D = 0.2917$).

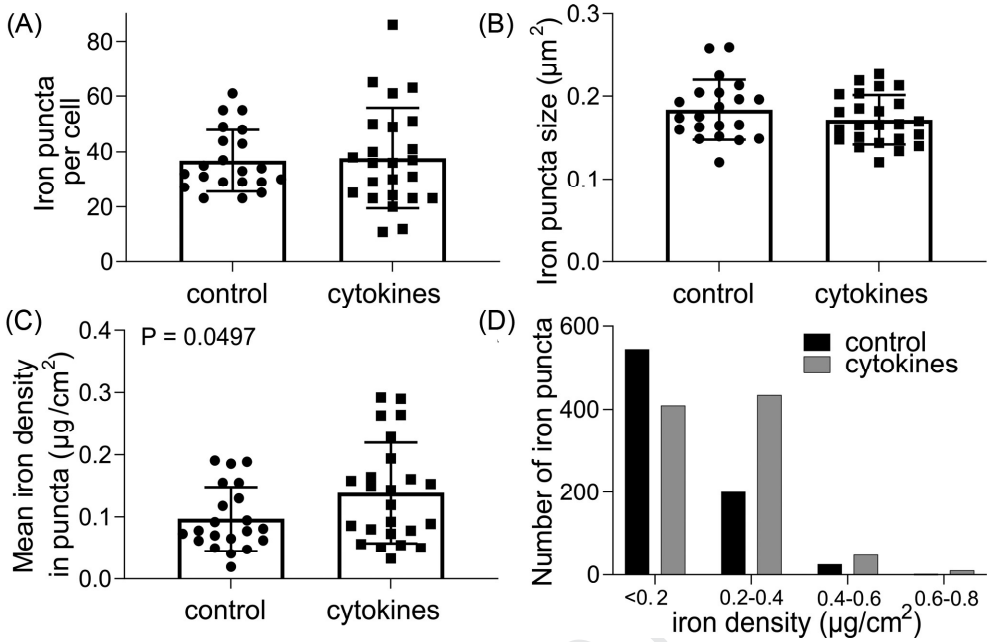

Fig. 2 The quantification and description of iron puncta quantified with ImageJ macro in single pancreatic beta-cells with or without 48-h exposure to cytokines (10pg/ml IL-1beta and 20pg/ml IL-6). The columns represent means ± S.D. Each dot represents the value of an individual beta-cell. N (control) = 21 cells; N (cytokines) = 24 cells. (A) The number of iron puncta in each cell. (B) The mean size of iron puncta in each cell. (C) The mean iron density in puncta in each cell. Two sample t-test, t(2.020) = 43, P = 0.0497, N(control) = 21 cells, N(cytokines) = 24 cells. (D) The frequency distribution of iron puncta with iron density. N(control) = 773 puncta, N(cytokines) = 904 puncta.

phosphatases, and calcium binding transcription factors involved with cytokine action and may indirectly regulate gene transcription as reported by Sabatini.[61] Finally, calcium has been reported in insulin granules of rat beta-cells[52] and insulin granules also occupy perinuclear space.

Iron in pancreatic beta-cells is localized to unique punctate structures which accumulate higher levels of iron after exposure to cytokines

Iron has been linked to the development of T2D because (1) a diet rich in iron is considered a risk factor for developing T2D,[62] (2) an increase in body stores of iron is associated with an increase in prevalence of T2D,[63,64] and (3) T2D is prevalent in patients with diseases of iron overload.[65] The damaging effects of iron can be explained by ferrous ion catalyzing the Fenton reaction resulting in formation of toxic reactive oxygen spices (ROS).[66] Utilizing SXFM estimated mean total cellular iron content was 30.4 ± 12.2 fg, and after exposure to cytokines was slightly increased to 47.2 ± 36.4 fg (mean ± S.D.) (Kolmogorov–Smirnov t-test, $P = 0.2965$, $D = 0.2917$, N (control) = 21, N (cytokines) = 24) (Fig. 1G). Although the mean total cellular iron content was not statistically different in beta-cells before and after exposure to cytokines, a subset of cells (38% of total observed cells) exhibited much higher iron contents after exposure to cytokines (Fig. 1G), suggesting that this subset of beta-cells accumulate iron during exposure to cytokines. These differences in total iron content suggest that beta-cells don't respond homogeneously to the cytokine exposure, which may be due to beta-cell heterogeneity, which is discussed further in the section—heterogeneity of beta-cell metallome.

Further analysis of SXFM images shows that iron is found throughout beta-cells and about 25% of cellular iron is localized to distinct puncta that are distributed throughout the cytosol (Fig. 1A, D). These concentrated iron puncta are similar to structures that have been reported previously in neurons,[29,40] however, the identity of the iron puncta in neurons and beta-cells remains unknown. Unlike the punctate distribution of zinc and calcium, the iron puncta in beta-cells appear as singular, defined structures that are mostly circular, and each iron punctum has a well-defined center (Fig. 1A). In untreated beta-cells, the mean number of iron puncta per cell was 36.8 ± 11.3 puncta and 37.7 ± 18.2 puncta per cell (mean ± S.D.) in cells after exposure to cytokines (Fig. 2A). The mean size of the iron puncta in untreated beta-cells was 0.184 ± 0.036 μm^2 and 0.172 ± 0.029 μm^2 (mean ± S.D.) in beta-cells after exposure to cytokines (Fig. 2B). The estimated iron density in puncta of untreated beta-cells is 0.097 ± 0.052 $\mu g/cm^2$ and 0.139 ± 0.081 $\mu g/cm^2$ (mean ± S.D.) in beta-cells after exposure to cytokines (Two sample t-test, t(2.02) = 43, $P = 0.0497$, N (control) = 21, N (cytokines) = 24) (Fig. 2C). In addition, when the iron density in each punctum was plotted as a frequency distribution, we observed an increased number of iron puncta with high mean density when compared to untreated cells ($\chi 2$ (3, N = 1674) = 109.0, $P < 0.0001$) (Fig. 2D). These data indicate that although there are no apparent changes in the mean total cellular iron content or mean number of puncta per cell after exposure to cytokines, iron accumulates to higher levels in a subset of iron puncta. Cellular iron accumulation contributes to ferroptosis, and ferroptosis has been recently linked to dysfunction of beta-cells under circumstances of T2D.[67] The sub-population of beta-cells that accumulates iron during cytokine exposure may be more susceptible to ferroptosis. In addition, we exposed cells to a low concentration of cytokines for a short duration, and the iron accumulation we observe may be the first stages of a longer-lasting response. It is possible that with prolonged exposure more cells would accumulate iron. Conversely, it is possible that iron accumulation in puncta is an adaptive response, and that iron is sequestered in these structures to protect cells from detrimental iron influence and warrants further investigation.

UNCORRECTED

COLOUR ONLINE, B&W IN PRINT

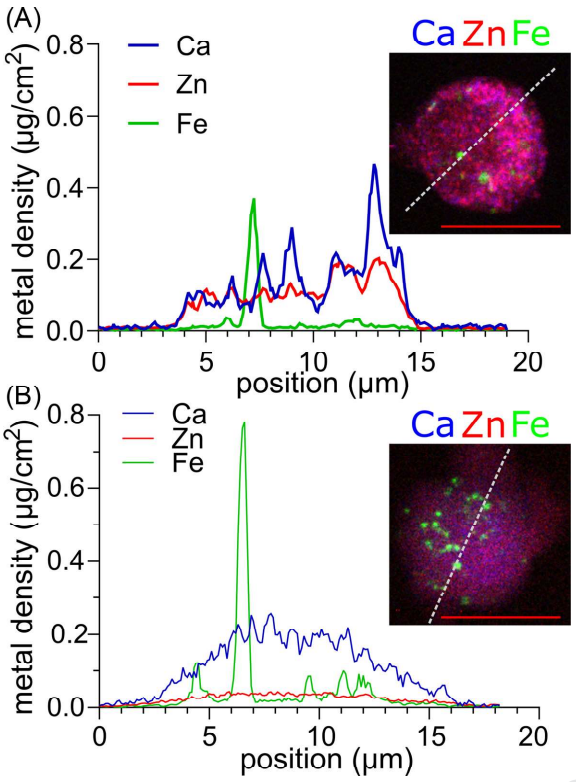

Fig. 3 Co-localization of zinc, calcium, and iron in pancreatic beta-cells with or without 48-h exposure to cytokines (10 pg/ml IL-1beta and 20 pg/ml IL-6) as detected by a line scan of SXFM images. The insert is a merged image of pseudo color: iron (green), zinc (red), and calcium (blue). Scale bar is 10 μm (red bar in the lower right corner of the insert). Zn (max = 0.2 μg/cm^2), Ca (max = 0.5 μg/cm^2), Fe (max = 0.25 μg/cm^2). The grey dotted line is the line scan position. (A). Densities of zinc, calcium, and iron in control beta-cell (untreated). (B) Densities of zinc, calcium, and iron in beta-cell after exposure to cytokines.

Co-localization and possible cross talk between zinc, calcium, and iron in pancreatic beta-cells

A unique aspect of SXFM analysis is the ability to simultaneously visualize multiple metals in the same cell, thus allowing the identification of areas of co-localization of metals. To visualize metal colocalization, lines scans of zinc, calcium, and iron are shown overlayed in Fig. 3A. This analysis shows the density of each metal as a function of location in the cell and relative to each other. This method can help identify co-localization of metals if the peak densities are found at the same position. The overlay of line scans of zinc and calcium shows peaks in the same cellular region, however, calcium and zinc peaks do not co-localize perfectly (Fig. 3A), suggesting that there may be distinct sites within beta-cells with high densities of either zinc or calcium. On the other hand, some peaks do appear to colocalize, which may correspond to localization to same organelle, however these data should be interpreted with caution, because the observed SXFM is a 2D projection of a 3D cellular structure and co-localization of 2D signals may not translate into co-localization of the metals in the cell. Nevertheless, zinc and calcium have been reported to co-localize in insulin granules of rat beta-cells,[52] however the granular calcium was reported to be labile and diffusible. After cells were exposed to cytokines zinc is markedly depleted relative to calcium (Fig. 3B). In addition, line scans reveal that regions with iron puncta (iron peaks) do not contain concentrations of zinc or calcium in either untreated or cytokine-challenged cells (Fig. 3A & B), suggesting that iron puncta are distinct iron-specific structures that accumulate iron and do not contain either calcium or zinc.

Heterogeneity of beta-cell metallome

Detailed observations of all scanned control cells revealed a heterogeneous metallome where a sub-group of cells exhibits high content of zinc, calcium, and iron, in contrast to other control cells with lower metal contents for the three metals (Fig. 4A). In the cytokine-treated group, all cells exhibited decreased zinc, however there were two groups in relation to calcium and iron (Fig. 4B). The first group of cells contained much higher iron than observed in any control cells along with higher calcium, while the second group contained lower calcium and iron (Fig. 4B). The heterogeneity of beta-cell metallome can be further seen when the total content of zinc, calcium, and iron are plotted for each beta-cell on a 3D scatter plot (Fig. 4C). In agreement with the visual observations, the control (untreated) beta-cells distribute into two distinct subsets: the majority of untreated beta-cells contains high calcium (>300 fg) and zinc (>50 fg) and low iron (<40 fg). A smaller subset of beta-cells contains lower concentrations of all three metals (Fig. 4C). These data suggest that there are at least two distinct metallome signatures in beta-cells. Interestingly, two different metallome signatures also are evident after exposure to cytokines, where most of the cytokine-treated beta-cells had depleted zinc (<50 fg), have reduced calcium (<250 fg) and unaltered iron (<40 fg) levels. There is a smaller subset of cytokine-treated beta-cells that have both high iron (>60 fg) and high calcium content (>200 fg).

The heterogeneity of beta-cells is a well-established concept, however the exact identity of the sub-population of beta-cells is an evolving and complex theory.[68–72] Customarily, beta-cells are subdivided into heterogeneous groups by insulin status, glucose metabolism, redox state, and membrane potential. Often these groups are identified by gene expression profiles and fluorescent probes. Our SXFM data of single beta-cell metallome suggest that there may be another angle of beta-cell heterogeneity that includes metal content. At this stage it is difficult to speculate if the metallome heterogeneity can be assigned to any identified beta-cell sub-populations. However, because we observed two distinct sub-population of beta-cell metallomes, it is possible that these differences reflect the mature vs. immature beta-cells described by Benninger and Hodson.[71] In addition, mature beta-cells perform the proper function of insulin secretion, for which both zinc and calcium are required. Conversely, it is possible that exposure to cytokines may shift the beta-cell phenotype into transdifferentiated or de-differentiated states and is an interesting avenue of further research

Conclusions

Cytokine concentrations seen in low-grade inflammation occurring with obesity, when applied to beta-cells in primary culture does not result in their death as we have shown previously.[10,13] In contrast, the investigation of the beta-cell metallome, after exposure to the same concentrations of cytokines, shows that there are striking changes to the total cellular contents and distributions of zinc and calcium and observable changes to the distribution of iron, demonstrating noteworthy changes to metal homeostatic processes are occurring in pancreatic beta-cells during cytokine exposure. These changes may not affect cell function and survival short-term; they may even be part of the normal adaptive cellular response. Interestingly, it has been reported recently that

UNCORRECTED PROOF

COLOUR ONLINE, B&W IN PRINT

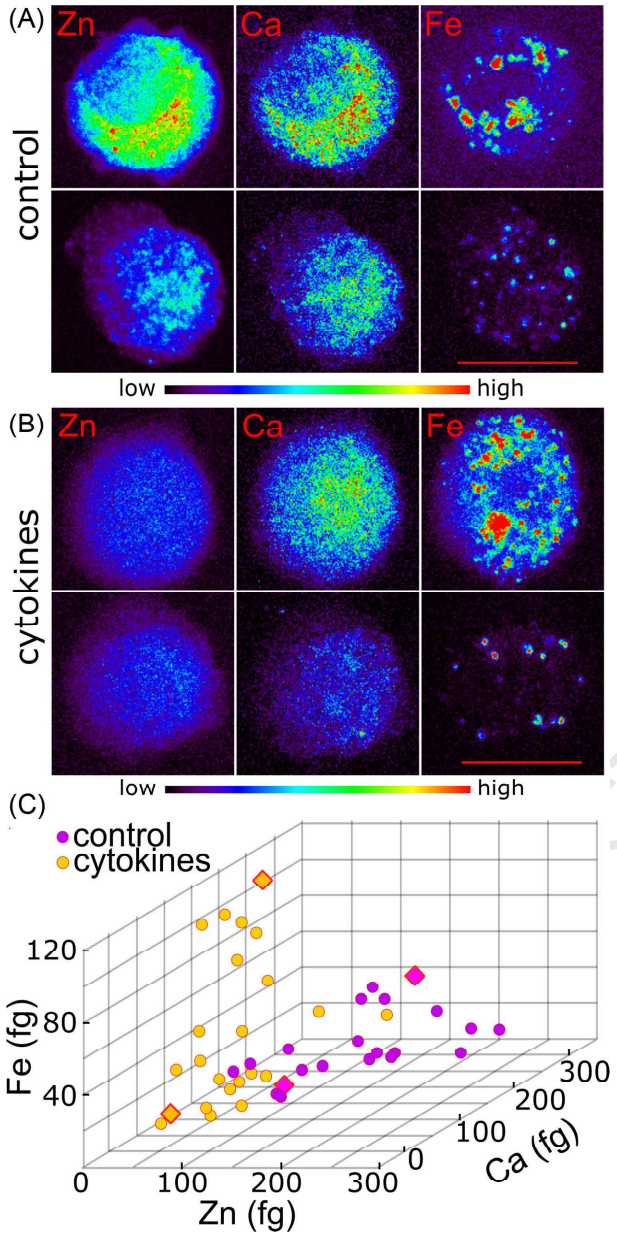

Fig. 4 Heterogeneity of beta-cell metallome. (A) Representative images of control (untreated) cells with high metal content (top) or low metal content (bottom). Zn (max = 0.4 $\mu g/cm^2$), Ca (max = 0.5 $\mu g/cm^2$), Fe (max = 0.25 $\mu g/cm^2$). (B) Representative images of cells after 48-h exposure to cytokines (10 pg/ml IL-1beta and 20 pg/ml IL-6). Top row displays a cytokine-treated cell with high iron content; bottom row displays a cell with low metal content. Zn (max = 0.2 $\mu g/cm^2$), Ca (max = 0.5 $\mu g/cm^2$), Fe (max = 0.25 $\mu g/cm^2$). Scale bar 10 μm (red bar in the lower right corner). (C) 3D-scatter plot of total metal contents. Each point represents total content (fg) of zinc, calcium, and iron in one beta-cell (N(control) = 21 cells, N(cytokines) = 24 cells). The cells presented in panels A and B are resented as diamond shapes on the scatter plot.

short-term exposure to cytokines has protective influence by up-regulating expression of protective genes.[73] However, after chronic exposure to inflammation, as seen in obese individuals, persistent disruption of metal homeostatic processes that we have observed will likely contribute to cell dysfunction and development of T2D and warrants further investigation. Data obtained by SXFM provide a unique opportunity to study such metallomic processes in pancreatic beta-cells. The data presented in the study was obtained from male beta-cells and further investigation of female beta-cells is of interest to determine if there are sex differences in the metallome of beta-cells and their response to cytokines.

In addition, we show that SXFM is a sensitive and appropriate tool to determine changes in the metallome of pancreatic beta-cells, thus it can be utilized to investigate not only cytokine exposure but other conditions, which will contribute to a better understanding of beta-cell function.

Supplementary material

Supplementary data are available at *Metallomics* online.

Acknowledgments

We want to thank Advanced Photon Source scientists Dr Barry Lai for providing training and helpful discussion about synchrotron radiation and scanning the hydrated cells with 2-ID-D beamline; Dr Qiaoling Jin for help with cell fixation, and helpful discussions about experimental set up and optimization; and Mr Evan Maxey for support at the beamline. We thank Dr Sarah Wyatt for critical discussion about manuscript layout and for critical review of the early drafts of the manuscript. This research used resources of the Advanced Photon Source, a U.S. Department of Energy (DOE) Office of Science User Facility, operated for the DOE Office of Science by Argonne National Laboratory under Contract No. DE-AC02-06CH11357. Extraordinary facility operations were supported in part by the DOE Office of Science through the National Virtual Biotechnology Laboratory, a consortium of DOE national laboratories focused on the response to COVID-19, with funding provided by the Coronavirus CARES Act.

Funding

This work was funded by the Ohio University Heritage College of Osteopathic Medicine and Osteopathic Heritage Foundation based on work originally funded by the NIH (R01 DK089182). Additional funding was provided by R15 DK121247.

Data Availability

The data underlying this article are available in the article and in its online supplementary material.

Conflicts of interest

There are no conflicts to declare.

References

1. National Diabetes Statistics Report 2020, *Estimates of diabetes and its burden in the United States*, 2020, 32.
2. C. S. Nunemaker, Considerations for defining cytokine dose, duration, and milieu that are appropriate for modeling chronic low-grade inflammation in type 2 diabetes, *J. Diabetes Res.*, 2016, 2016, 2846570.
3. E. U. Alejandro, B. Gregg, M. Blandino-Rosano, C. Cras-Méneur and E. Bernal-Mizrachi, Natural history of β-cell adaptation and failure in type 2 diabetes, *Mol. Aspects Med.*, 2015, 42, 19–41.
4. X. Wang, W. Bao, J. Liu, Y. Y. Ouyang, D. Wang, S. Rong, X. Xiao, Z. L. Shan, Y. Zhang, P. Yao and L. G. Liu, Inflammatory markers and risk of type 2 diabetes, *Diabetes Care.*, 2013, 36 (1), 166–175.

5. J. Spranger, A. Kroke, M. Möhlig, K. Hoffmann, M. M. Bergmann, M. Ristow, H. Boeing and A. F. Pfeiffer, Inflammatory cytokines and the risk to develop type 2 diabetes: results of the prospective population-based european prospective investigation into cancer and nutrition (epic)-Potsdam Study, *Diabetes*, 2003, 52 (3), 812–817.
6. A. D. Pradhan, J. E. Manson, N. Rifai, J. E. Buring and P. M. Ridker, C-Reactive protein, interleukin 6, and risk of developing type 2 diabetes mellitus, *JAMA*, 2001, 286 (3), 327–334.
7. K. Alexandraki, C, Piperi, C, Kalofoutis, J, Singh, A, Alaveras, A and Kalofoutis, Inflammatory process in type 2 diabetes, *Ann. N. Y. Acad. Sci.*, 2006, 1084 (1), 89–117.
8. K. E. Wellen and G. S. Hotamisligil, Inflammation, stress, and diabetes, *J. Clin. Invest.*, 2005, 115 (5), 1111–1119.
9. H. Kolb and T. Mandrup-Poulsen, The global diabetes epidemic as a consequence of lifestyle-induced low-grade inflammation, *Diabetologia*, 2010, 53 (1), 10–20.
10. C. M. O'Neill, C. Lu, K. L. Corbin, P. R. Sharma, S. B. Dula, J. D. Carter, J. W. Ramadan, W. Xin, J. K. Lee and C. S. Nunemaker, Circulating levels of IL-1B+IL-6 cause ER stress and dysfunction in islets from prediabetic male mice, *Endocrinology*, 2013, 154 (9), 3077–3088.
11. F. M. Qureshi, E. A. Dejene, K. L. Corbin and C. S. Nunemaker, Stress-induced dissociations between intracellular calcium signaling and insulin secretion in pancreatic islets, *Cell Calcium*, 2015, 57 (5-6), 366–375.
12. P. Jahanshahi, R. Wu, J. D. Carter and C. S. Nunemaker, Evidence of diminished glucose stimulation and endoplasmic reticulum function in nonoscillatory pancreatic islets, *Endocrinology*, 2009, 150 (2), 607–615.
13. S. B. Dula, M. Jecmenica, R. Wu, P. Jahanshahi, G. M. Verrilli, J. D. Carter, K. L. Brayman and C. S. Nunemaker, Evidence that low-grade systemic inflammation can induce islet dysfunction as measured by impaired calcium handling, *Cell Calcium*, 2010, 48 (2-3), 133–142.
14. K. L. Corbin, T. E. Hall, R. Haile and C. S. Nunemaker, A novel fluorescence imaging approach for comparative measurements of pancreatic islet function in vitro, *Islets*, 2011, 3 (1), 14–20.
15. A. T. Templin, M. Mellati, D. T. Meier, N. Esser, M. F. Hogan, J. J. Castillo, R. Akter, D. P. Raleigh, S. Zraika, R. L. Hull and S. E. Kahn, Low concentration IL-1β promotes islet amyloid formation by increasing hIAPP release from humanised mouse islets in vitro, *Diabetologia*, 2020, 63 (11), 2385–2395.
16. N. R. Johnston, R. K. Mitchell, E. Haythorne, M. P. Pessoa, F. Semplici, J. Ferrer, L. Piemonti, P. Marchetti, M. Bugliani, D. Bosco, E. Berishvili, P. Duncanson, M. Watkinson, J. Broichhagen, D. Trauner, G. A. Rutter and D. J. Hodson, Beta cell hubs dictate pancreatic islet responses to glucose, *Cell Metab.*, 2016, 24 (3), 389–401.
17. N. L. Farnsworth, R. L. Walter, A. Hemmati, M. J. Westacott and R. K. P. Benninger, Low level pro-inflammatory cytokines decrease connexin36 gap junction coupling in mouse and human islets through nitric oxide-mediated protein kinase Cδ, *J. Biol. Chem.*, 2016, 291 (7), 3184–3196.
18. M. Lytrivi, M. Igoillo-Esteve and M. Cnop, Inflammatory stress in islet β-cells: therapeutic implications for type 2 diabetes? *Curr. Opin. Pharmacol.*, 2018, 43, 40–45.
19. R. S. Ohgami, D. R. Campagna, A. McDonald and M. D. Fleming, The Steap proteins are metalloreductases, *Blood*, 2006, 108 (4), 1388–1394.
20. P. R. Sharma, A. J. Mackey, E. A. Dejene, J. W. Ramadan, C. D. Langefeld, N. D. Palmer, K. D. Taylor, L. E. Wagenknecht, R. M. Watanabe, S. S. Rich and C. S. Nunemaker, An islet-targeted genome-wide association scan identifies novel genes implicated in cytokine-mediated islet stress in type 2 diabetes, *Endocrinology*, 2015, 156 (9), 3147–3156.
21. L. Egefjord, J. L. Jensen, C. H. Bang-Berthelsen, A. B. Petersen, K. Smidt, O. Schmitz, A. E. Karlsen, F. Pociot, F. Chimienti, J. Rungby and N. E. Magnusson, Zinc transporter gene expression is regulated by pro-inflammatory cytokines: a potential role for zinc transporters in beta-cell apoptosis?, *BMC Endocr Disord.*, 2009, 9 (1), 7.
22. S. Lortz, S. Schröter, V. Stückemann, I. Mehmeti and S. Lenzen, Influence of cytokines on Dmt1 iron transporter and ferritin expression in insulin-secreting cells, *J. Mol. Endocrinol.*, 2014, 52 (3), 301–310.
23. A. K. Cardozo, F. Ortis, J. Storling, Y. M. Feng, J. Rasschaert, M. Tonnesen, F. Van Eylen, T. Mandrup-Poulsen, A. Herchuelz and D. L. Eizirik, Cytokines downregulate the sarcoendoplasmic reticulum pump Ca2+ ATPase 2b and deplete endoplasmic reticulum Ca2+, leading to induction of endoplasmic reticulum stress in pancreatic beta-cells, *Diabetes*, 2005, 54 (2), 452–461.
24. V. Aburto-Luna, S. Treviño, G. Santos-López, D. Moroni-González, O. Calva-Cruz, P. Aguilar-Alonso, B. A. León-Chávez and E. Brambila, Hepatic mobilization of zinc after an experimental surgery, and its relationship with inflammatory cytokines release, and expression of metallothionein and Zip14 transporter, *Inflamm. Res.*, 2017, 66 (2), 167–175.
25. R. Zhang, L. Li, Y. Sultanbawa and Z. P. Xu, X-ray fluorescence imaging of metals and metalloids in biological systems, *Am. J. Nucl. Med. Mol. Imaging*, 2018, 8, 169–188.
26. B. D. Samber, M. Bensellam, S. J. Van Malderen, F. Seiboth, D. Brückner, J. Garrevoet, G. Falkenberg, J. C. Jonas and L. Vincze, Proof-of-concept for 2D/CT element analysis of entire cryofrozen islets of Langerhans using a cryoloop synchrotron X-ray fluorescence setup, *J. Anal. At. Spectrom.*, 2020, 35 (7), 1368–1379.
27. J. D. Carter, S. B. Dula, K. L. Corbin, R. Wu and C. S. Nunemaker, A practical guide to rodent islet isolation and assessment, *Biol. Proced Online*, 2009, 11 (1), 3–31.
28. R. Zamora, Y. Vodovotz and T. R. Billiar, Inducible nitric oxide synthase and inflammatory diseases, *Mol. Med.*, 2000, 6 (5), 347–373.
29. R. A. Colvin, B. Lai, W. R. Holmes and D. Lee, Understanding metal homeostasis in primary cultured neurons. Studies using single neuron subcellular and quantitative metallomics, *Metallomics*, 2015, 7 (7), 1111–1123.
30. L. A. Finney and Q. Jin, Preparing adherent cells for X-ray fluorescence imaging by chemical fixation, *Journal of Visualized Experiments*, 2015, (97), 52370. doi:10.3791/52370.
31. S. Matsuyama, M., Shimura, M., Fujii, K., Maeshima, H., Yumoto, H., Mimura, Y and Sano. Elemental mapping of frozen-hydrated cells with cryo-scanning X-ray fluorescence microscopy, *X-Ray Spectrom.*, 2010, 39 (4), 260–266.
32. Q. Jin, T. Paunesku, B. Lai, S. C. Gleber, S. I. Chen, L. Finney, D. Vine, S. Vogt, G. Woloschak and C. Jacobsen, Preserving elemental content in adherent mammalian cells for analysis by synchrotron-based x-ray fluorescence microscopy, *J. Microsc.*, 2017, 265 (1), 81–93.
33. S. Chen, J. Deng, Y. Yuan, C. Flachenecker, R. Mak, B. Hornberger, Q. Jin, D. Shu, B. Lai, J. Maser, C. Roehrig, T. Paunesku, S. C. Gleber, D. J. Vine, L. Finney, J. VonOsinski, M. Bolbat, I. Spink, Z. Chen, J. Steele, D. Trapp, J. Irwin, M. Feser, E. Snyder, K. Brister, C. Jacobsen, G. Woloscha and S. Vogt, The Bionanoprobe: hard X-ray fluorescence nanoprobe with cryogenic capabilities, *J. Synchrotron Radiat.*, 2014, 21 (1), 66–75.

UNCORRECTED PROOF

34. J. Dolenšek, M. S. Rupnik and A. Stožer, Structural similarities and differences between the human and the mouse pancreas, *Islets*, 2015, 7 (1), e1024405.
35. R. T. Scarl, K. L. Corbin, N. W. Vann, H. M. Smith, L. S. Satin, A. Sherman and C. S. Nunemaker, Intact pancreatic islets and dispersed beta-cells both generate intracellular calcium oscillations but differ in their responsiveness to glucose, *Cell Calcium*, 2019, 83, 102081.
36. S. Vogt, MAPS : a set of software tools for analysis and visualization of 3D X-ray fluorescence data sets, *J. Phys. IV France*, 2003, 104, 635–638.
37. C. A. Schneider, W. S. Rasband and K. W. Eliceiri, NIH Image to ImageJ: 25 years of image analysis, *Nat. Methods*, 2012, 9 (7), 671–675.
38. H. J. Motulsky and R. E. Brown, Detecting outliers when fitting data with nonlinear regression – a new method based on robust nonlinear regression and the false discovery rate, *BMC Bioinformatics*, 2006, 7 (1), 123.
39. T. Bock, K. Svenstrup, B. Pakkenberg and K. Buschard, Unbiased estimation of total beta-cell number and mean beta-cell volume in rodent pancreas, *APMIS*, 1999, 107 (7-12), 791–799.
40. R. A. Colvin, Q. Jin, B. Lai and L. Kiedrowski, Visualizing metal content and intracellular distribution in primary hippocampal neurons with synchrotron X-Ray fluorescence, *PLoS One*, 2016, 11.
41. R. A. Colvin, A. I. Bush, I. Volitakis, C. P. Fontaine, D. Thomas, K. Kikuchi and W. R. Holmes, Insights into Zn2+ homeostasis in neurons from experimental and modeling studies, *Am J Physiol Cell Physiol.*, 2008, 294 (3), C726–C742.
42. A. Krezel and W. Maret, Zinc-buffering capacity of a eukaryotic cell at physiological pZn, *J Biol Inorg Chem.*, 2006, 11 (8), 1049–1062.
43. E. A. Bellomo, G. Meur and G. A. Rutter, Glucose regulates free cytosolic Zn2+ concentration, Slc39 (ZiP), and metallothionein gene expression in primary pancreatic islet β-Cells*, *J. Biol. Chem.*, 2011, 286 (29), 25778–25789.
44. R. Lawson, W. Maret and C. Hogstrand, Prolonged stimulation of insulin release from MIN6 cells causes zinc depletion and loss of β-cell markers, *J. Trace Elem. Med. Biol.*, 2018, 49, 51–59.
45. M. Bensellam, D. R. Laybutt and J. - C. Jonas, The molecular mechanisms of pancreatic β-cell glucotoxicity: recent findings and future research directions, *Mol. Cell. Endocrinol.*, 2012, 364 (1-2), 1–27.
46. M. E. Muayed, L. K. Billings, M. R. Raja, X. Zhang, P. J. Park, M. V. Newman, D. B. Kaufman, T. V. O'Halloran and W. L. Lowe, Jr, Acute cytokine-mediated downregulation of the zinc transporter ZnT8 alters pancreatic β-cell function, *J. Endocrinol.*, 2010, 206 (2), 159.
47. C. Merriman and D. Fu, Down-regulation of the islet-specific zinc transporter-8 (ZnT8) protects human insulinoma cells against inflammatory stress, *J. Biol. Chem.*, 2019, 294 (45), 16992–17006.
48. C. Talchai, S. Xuan, H. V. Lin, L. Sussel and D. Accili, Pancreatic β cell dedifferentiation as a mechanism of diabetic β cell failure, *Cell*, 2012, 150 (6), 1223–1234.
49. C. S. Hunter and R. W. Stein, Evidence for loss in identity, dedifferentiation, and trans-differentiation of islet β-cells in type 2 diabetes, *Front Genet*, 2017, 8, 35.
50. M. A. Atkinson and N. K. Maclaren, Islet cell autoantigens in insulin-dependent diabetes, *J. Clin. Invest.*, 1993, 92 (4), 1608–1616.
51. J. C. Hutton, E. J. Penn and M. Peshavaria, Low-molecular-weight constituents of isolated insulin-secretory granules. Bivalent cations, adenine nucleotides and inorganic phosphate, *Biochem. J.*, 1983, 210 (2), 297–305.
52. M. C. Foster, R. D. Leapman, M. X. Li and I. Atwater, Elemental composition of secretory granules in pancreatic islets of Langerhans, *Biophys. J.*, 1993, 64 (2), 525–532.
53. Q. Lu, H. Haragopal, K. G. Slepchenko, C. Stork and Y. V. Li, Intracellular zinc distribution in mitochondria, ER and the Golgi apparatus, *Int J Physiol Pathophysiol Pharmacol*, 2016, 8, 35–43.
54. L. Eliasson, F. Abdulkader, M. Braun, J. Galvanovskis, M. B. Hoppa and P. Rorsman, Novel aspects of the molecular mechanisms controlling insulin secretion, *J. Physiol.*, 2008, 586 (14), 3313–3324.
55. O. Idevall-Hagren and A. Tengholm, Metabolic regulation of calcium signaling in beta cells, *Semin. Cell Dev. Biol.*, 2020, 103, 20–30.
56. M. J. Berridge, The endoplasmic reticulum: a multifunctional signaling organelle, *Cell Calcium*, 2002, 32 (5-6), 235–249.
57. M. T. Dickerson, A. M. Bogart, M. K. Altman, S. C. Milian, K. L. Jordan, P. K. Dadi and D. A. Jacobson, Cytokine-mediated changes in K+ channel activity promotes an adaptive Ca2+ response that sustains β-cell insulin secretion during inflammation, *Sci. Rep.*, 2018, 8 (1), 1158.
58. A. L. Clark, K. Kanekura, Z. Lavagnino, L. D. Spears, D. Abreu, J. Mahadevan, T. Yagi, C. F. Semenkovich, D. W. Piston and F. Urano, Targeting cellular calcium homeostasis to prevent cytokine-mediated beta cell death, *Sci. Rep.*, 2017, 7 (1), 5611.
59. I. Quesada, F. Martin, E. Roche and B. Soria, Nutrients induce different Ca2+ signals in cytosol and nucleus in pancreatic -cells, *Diabetes*, 2004, 53 (Supplement 1), S92–S95.
60. J. W. Ramadan, S. R. Steiner, C. M. O'Neill and C. S. Nunemaker., The central role of calcium in the effects of cytokines on beta-cell function: Implications for type 1 and type 2 diabetes, *Cell Calcium*, 2011, 50 (6), 481–490.
61. P. V. Sabatini, T. Speckmann and F. C. Lynn, Friend and foe: β-cell Ca2+ signaling and the development of diabetes, *Mol Metab*, 2018, 21, 1–12.
62. K. Jomova and M. Valko, Advances in metal-induced oxidative stress and human disease, *Toxicology*, 2011, 283 (2-3), 65–87.
63. A. Aregbesola, S. Voutilainen, J. K. Virtanen, J. Mursu and T. - P. Tuomainen, Body iron stores and the risk of type 2 diabetes in middle-aged men, *Eur. J. Endocrinol.*, 2013, 169 (2), 247–253.
64. A. Aregbesola, S. Voutilainen, J. K. Virtanen, J. Mursu and T. - P. Tuomainen, Gender difference in type 2 diabetes and the role of body iron stores, *Biochem.*, 2017, 54 (1), 113–120.
65. J. A. Simcox and D. A. McClain, Iron and diabetes risk, *Cell Metab.*, 2013, 17 (3), 329–341.
66. C. C. Winterbourn, Toxicity of iron and hydrogen peroxide: the Fenton reaction, *Toxicol. Lett.*, 1995, 82-83, 969–974.
67. D. Li, C. Jiang, G. Mei, Y. Zhao, L. Chen, J. Liu, Y. Tang, C. Gao and P. Yao, Quercetin alleviates ferroptosis of pancreatic β cells in type 2 diabetes, *Nutrients*, 2020, 12 (10), 2954.
68. D. G. Pipeleers, Heterogeneity in pancreatic β-cell population, *Diabetes*, 1992, 41 (7), 777–781.
69. D. Avrahami, A. Klochendler, Y. Dor and B. Glaser, Beta cell heterogeneity: an evolving concept, *Diabetologia*, 2017, 60 (8), 1363–1369.
70. G. D. Gutierrez, J. Gromada and L. Sussel, Heterogeneity of the pancreatic beta cell, *Front. Genet.*, 2017, 8, 22.
71. R. K. P. Benninger and D. J. Hodson, New understanding of β-cell heterogeneity and in situ islet function, *Diabetes*, 2018, 67 (4), 537–547.
72. L. Farack, M. Golan, A. Egozi, N. Dezorella, K. Bahar Halpern, S. Ben-Moshe, I. Garzilli, B. Tóth, L. Roitman, V. Krizhanovsky and S. Itzkovitz, Transcriptional heterogeneity of beta cells in the intact pancreas, *Dev. Cell*, 2019, 48 (1), 115–125 e4.
73. J. S. Stancill, M. Y. Kasmani, A. Khatun, W. Cui and J. A. Corbett, Single-cell RNA sequencing of mouse islets exposed to proinflammatory cytokines, *Life Sci Alliance*, 2021, 4 (6), e202000949.

UNCORRECTED PROOF